Modeling steep-slope flow across staggered emergent cylinders: application to fish passes

Jacques Chorda, Ludovic Cassan, Pascale Laurens

Modeling Steep-Slope Flow across Staggered Emergent Cylinders: Application to Fish Passes

Jacques Chorda[1]; Ludovic Cassan[2]; and Pascale Laurens[3]

Abstract: Designing efficient rock ramp fish passes with flows over a bottom with roughness on the same scale as the water depth requires a precise knowledge of hydrodynamics in order to avoid or limit characteristics unattractive for fish, particularly for small fish. This paper considered the numerical modeling of free surface flow across a steep sloped ramp covered with staggered surface emergent cylinders. Considering the importance of complex flow features for fish passage, computational fluid dynamics (CFD) was adopted because it is capable of predicting such features. Because of the longitudinal periodicity of the arrangement of the obstacles, cyclic boundary conditions made this fine simulation possible. Two computational meshes (coarse and fine) and two turbulence models [shear stress transport (SST) $k\ \omega$ and Smagorinsky large eddy simulation (LES)] were used. The SST $k\ \omega$ coarse mesh model gives correct time averaged values, the main flow unstationarities and is usable for rock ramp fish pass design, but a fine model using LES turbulence closure can provide detailed flow characteristics in the wakes in order to provide possible rest zones, particularly for smaller fish.

Introduction

A rock ramp fish pass generally consists of a sloped bottom covered with a periodic array of staggered obstacles designed to control the dissipated energy. Free surface flows across such an ar rangement of obstacles are of great complexity because they asso ciate flow separation around obstacles and wake interactions conjugated with transcritical zones due to the steep longitudinal slope. Dominant characteristics of these flows are an agitated free surface, strong velocity fluctuations, and formation of local dipha sic zones. Instabilities are frequently observed in the wakes, and the three dimensional (3D) nature of such flows appears as dominant (interactive wakes and horseshoe vortex). They have been investi gated by many authors experimentally (Nepf et al. 1997; Graf and Istiarto 2010; Zhou et al. 2002; Kirkil et al. 2008; Breton et al. 2013; Baki et al. 2014a, b; Tran et al. 2016; Baki et al. 2017) and numerically (Tseng et al. 2000; Kawamura et al. 2002; Hinterberger et al. 2007; Yu et al. 2008; Shao et al. 2013; Baki et al. 2016; Tran et al. 2016). Tran et al. (2016) conducted flume experiments at the Institut de Mécanique des Fluides de Toulouse (IMFT), but a serious limitation resulted from the flow character istics: shallow water depths similar to the diameter of the blocks, proximity of obstacles limiting probe placement, free surface agi tation, and diphasic air water occurrences. Consequently, measure ments using acoustic Doppler velocimeter (ADV) probes or optical methods are difficult and do not allow a complete description of flow. Numerical modeling can give detailed information provided that its results are validated by comparison with measurement data. However, efficient 3D free surface flow modeling necessitates us ing very fine meshes, and free surface resolution drastically in creases the computation time. In order to reduce this time for hydraulic engineering purposes and to test several configurations, Tran et al. (2016) used the two dimensional (2D) shallow water code TELEMAC 2D (Hervouet 2007). Tran showed that this 2D modeling gives acceptable mean values of velocities and reveals its limitations, particularly when the Froude number exceeds 0.7. The discrepancies are due to shallow water hypothesis equa tions such as hydrostatic pressure distribution and moreover to the intrinsic nature of the considered flows. Baki et al. (2016) simulated a 3D rock ramp fish pass using ANSYS CFX commercial software with the volume of fluid (VOF) method. The geometry of the de sign was a staggered pattern of quasi spherical boulders. Various slopes, discharges, and submergence ratios were tested, thus ena bling relationships to calculate water depth and velocity as a func tion of discharge. Baki et al. assessed flow resistance and gave optimized boulder spacing for fish passage. The turbulence closure was the classical $k\ \varepsilon$, which is not a priori the most suitable for detached flows (Menter et al. 2003) such as those encountered here. Ducrocq et al. (2017), using a single surface piercing cylinder, demonstrated that the OpenFOAM toolbox allowed 3D free surface flow numerical modeling using the VOF method (interFoam solver), with numerical results conforming to experiments per formed at IMFT. Ducrocq et al. (2017) demonstrated that the shear stress transport (SST) $k\ \omega$ model (Menter 1994) was well fitted to the unsteady Reynolds averaged Navier Stokes (URANS) simula tion, but that large eddy simulation (LES) can afford a significant improvement in the physics of flow modeling despite increased computation cost (Ducrocq 2016). Silva et al. (2012), who studied the swimming behavior of cyprinids in response to turbulent flow, concluded that "there is a strong gap between the spatial and tem poral resolution of flows at which hydraulics are modelled and at which fish respond," necessitating the use of CFD to "allow a more comprehensive understanding of physical phenomena, as well as predict and analyze the levels of turbulence in unsteady flows."

The main purpose of this paper, considering the importance of complex flow features for fish passage, was to show that CFD can predict complex flow features using certain mesh resolution and

[1]Fluid Mechanics Dept. Laboratory, Institut de Mécanique des Fluides, Allée du Professeur Camille Soula, Toulouse 31400, France (corresponding author). Email: chorda@imft.fr

[2]Fluid Mechanics Dept. Laboratory, Institut de Mécanique des Fluides, Allée du Professeur Camille Soula, Toulouse 31400, France. Email: lcassan@imft.fr

[3]Fluid Mechanics Dept. Laboratory, Institut de Mécanique des Fluides, Allée du Professeur Camille Soula, Toulouse 31400, France. Email: pascale.laurens@imft.fr

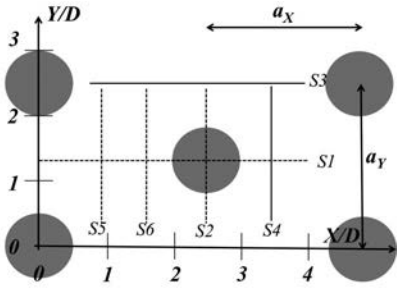

Fig. 1. Notations and ADV measurement profile locations in a fully developed flow zone by Tran et al. (2016).

turbulence models. This implies finely modeling a staggered con figuration of unsubmerged cylinders in order to consider the most detailed flow features relevant to fish passage, even for small spe cies. The periodicity of the arrangement of cylinders makes it pos sible to apply cyclic boundary conditions at inlet and outlet sections, and consequently to reduce the modeled length, making this fine simulation possible. We first describe the former experi mental setup used by Tran et al. (2016), then the numerical model building using OpenFOAM version 4.1 and the adaptation made to apply cyclic boundary conditions. Two meshes with different den sities and extents were tested. For turbulence closure, two models suitable for detached flows with recirculation were used (Ducrocq et al. 2017): URANS SST k ω, and Smagorinsky LES. The results were validated by comparison with measurement data followed by an audit of these models, focusing on fish comfort. Lastly, with application for fish passage in mind, the model based upon the fine mesh and LES was rescaled in order to simulate flow in a fishway at prototype scale. Flow criteria compatible with fish are discussed for the configuration used here, paying particular attention to potential rest zones.

Description of Previous Experiments

Experimental data were taken from the tests conducted by Tran et al. (2016) in a tilting flume. The channel was $B = 1$ m wide and 7 m long, supplied with water by a centrifugal pump with a maximum discharge of 0.1 m^3s^{-1}. The obstacles (wooden cylinders with diameter = 0.115 m and height = 0.15 m) were regularly staggered and distributed along 24 longitudinal rows at a concentration $C =$ 16% on a smooth steel bottom. The concentration C is the ratio $D^2/a_X a_Y$, where a_X and a_Y are the distances between blocks in the longitudinal and transverse directions respectively (Fig. 1). With $C = 16\%$ and ($a_X = a_Y = 0.285$ m), the relative block spac ing $a_x/D = 2.5$ corresponds to the range proposed by Baki et al. (2016). Velocity profile measurements were performed using an acoustic Doppler velocimeter with a 3D downlooking probe giving the three velocity components (u, v, and W) at a sampling rate of 50 Hz. After despiking the raw ADV signal, the values U, V, and W correspond to time averaged measurements over 180 s. The aver aged water depth h was obtained by shadowgraphy using a 2K*2K video camera (Cassan et al. 2014). The lateral averaged free surface position was measured with a frequency of 3 Hz, and 600 pictures were averaged and integrated in the longitudinal direction to get the water depth. The reference configuration is defined in this paper using the following values: concentration $C = 16\%$, discharge $Q = 0.05$ m^3s^{-1}, and slope $S = 5\%$. This configuration corre sponds to a condition with unsubmerged obstacles. The ADV mea surements were performed at $z = 0.04$ m above the bottom at

Table 1. Hydraulic conditions for numerical tests

Characteristics	Values
Concentration, C (%)	16
Slope, S (%)	5
Width, B (m)	1
Water discharge, Q (m^3s^{-1})	0.050
Bed surface	Smooth
Water height, h (mm)	100
Velocity between obstacles, V_g ($m \cdot s^{-1}$)	0.83
Froude number	0.83
Reynolds number	99,600

Note: Obstacle concentration and slope correspond to a possible fishway flow; flume width B and hydraulic data taken from experiments by Tran et al. (2016).

locations along the profiles in Fig. 1. This distance z avoided the bottom boundary effect appearing for $z < 0.03$ m (Chanson et al. 2007; Liu et al. 2002). The ADV downlooking probe obstruc tion could not perform measurements near blocks, and no ADV side looking probe was available. An averaged velocity V_g between blocks was calculated with Eq. (1) and used as reference velocity

$$\frac{V_g}{V_0} = \frac{1}{1 - \sqrt{\frac{a_Y}{a_X}}C} \tag{1}$$

where $V_0 = Q/(Bh)$ = bulk velocity.

The Froude number was $V_g/\sqrt{gh}$ and the Reynolds number was $V_g D/\nu$ (Cassan et al. 2014) (Table 1).

Numerical Modeling

Description of Modeled Domain and Meshes

Based upon a series of experiments in a fully developed flow zone by Tran et al. (2016), we retained the same configuration for numerical tests with a 1 m wide flume covered with a spatial con centration $C = 16\%$ of cylinders, a value commonly used for rock ramp fishways, and a longitudinal slope $S = 5\%$. This steep slope induced the relatively high Froude values which were of interest (Tseng et al. 2000). To test severe flow conditions, we reproduced hydrodynamics data obtained with discharge $Q = 0.050$ m^3s^{-1}. Because the interest was in a zone for which flow is said to be in a state of equilibrium with gravity balanced by resistance forces and friction losses, a pertinent choice, due to geometrical periodic ity of the blocks in the longitudinal direction, was to represent only a few elements of the pattern instead of the full length of the flume, which would have involved an unacceptable computational cost, and to apply cyclic boundary conditions at the inlet and outlet. Two models were tested: coarse Mesh1 representing a pattern with eight rows of obstacles (length = 2.28 m, and width = 1 m) and fine Mesh2, limited to four rows of obstacles (length = 1.14 m, and width = 1 m) (Fig. 2). It was not necessary to represent more than one pattern (two rows), but doing so enabled us to observe flow setup around the obstacles and the interactions of wakes between rows. The meshes were built using the open source SALOME version 8.3 software platform. For free surface piercing obstacles, 3D meshes were obtained by vertical extrusion of a 2D mesh of triangular cells. As a result, the 3D generated meshes were composed of prismatic cells, well fitted to solving free surface wall bounded flows, because this technique maintains orthogonal grids in the wall normal direction (Lai et al. 2003). These meshes

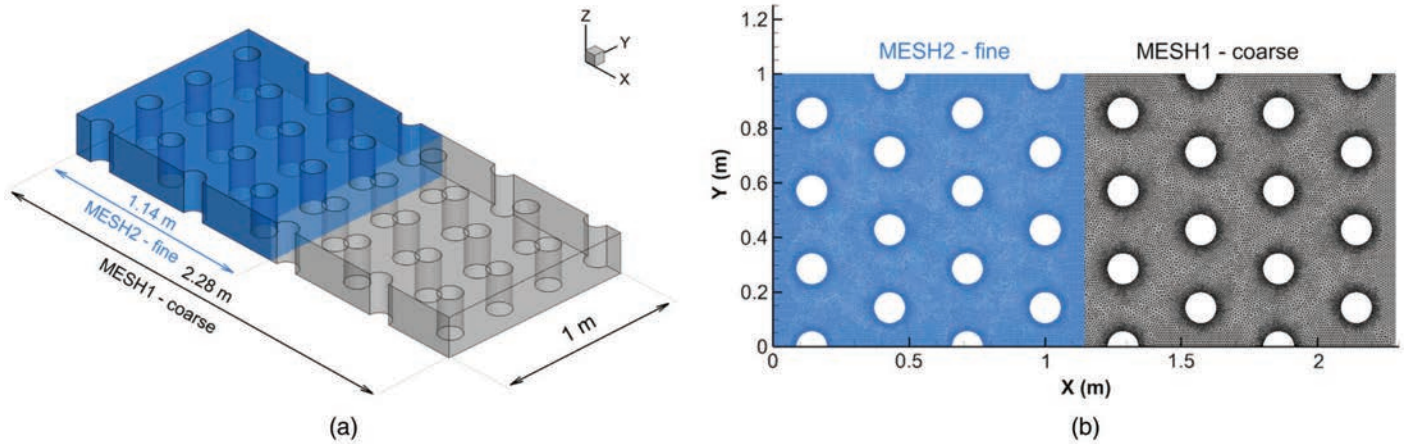

Fig. 2. (Color) Two computational domains corresponding to longitudinal portions of the flume experiments by Tran et al. (2016): (a) locations of coarse and fine meshes; and (b) extents of coarse and fine meshes.

Table 2. Coarse and fine mesh characteristics

Meshes characteristics	Mesh1 (coarse)	Mesh2 (fine)
2D model dimensions (m)	2.28×1	1.14×1
Maximum cell size (mm)	10	5
Local cell size (mm)	4	2
Number of vertical cells	50	75
Cell height (mm)	4	2
Model elevation (m)	0.20	0.15
Total number of 3D prismatic cells	4,300,000	8,600,000

Note: Meshes were built by vertical extrusion of a 2D unstructured triangular mesh; the fine mesh was about twice as fine as the coarse mesh.

were exported in IDEAS universal format (.unv) which can be im ported directly into OpenFOAM. Using cyclic mode in Open FOAM necessitated building inlet and outlet faces as perfect clones, which was obtained by including submeshes in SALOME. The bottom plane was horizontal ($Z = 0$) because the longitudinal slope effect was given by the $g\sin(\theta)$ gravity component with $\theta = \arctan(S)$. The two meshes were created with the characteris tics given in Table 2.

The cyclic mode significantly reduced the size of meshes and the computational cost, and also made finer modeling possible: a full length (7 m) flume mesh with classical boundary conditions would need about 48 million cells.

Adaptation for Cyclic Mode

First tests with OpenFOAM revealed a problem when using the cyclic mode: it appeared that cyclic inlet outlet boundary condi tions (BCs) do not work using the original two phase VOF inter Foam solver. The problem is because usual BC prescriptions were simplified in OpenFOAM version 4.1 by solving the $p - \rho gZ$ term instead of pressure p. Cyclic BCs work well for internal flows but not for free surface flows. It therefore was necessary to separate the gravity term from dynamic pressure and add it back into the mo mentum equation. Because the software was open source, we were able to make slight modifications to the interFoam code to suppress this limitation regarding free surface flow; details of this modifica tion are included in the Supplemental Data. The numerical model represented a period of a few patterns with cyclic BCs at inlet and outlet sections. Cyclic BCs avoid the standard flow discharge imposition at inlet with an arbitrary velocity distribution and a zero gradient at outlet (free condition) or a pressure field corresponding to an imposed water depth. Unlike classical BCs, the turbulent kinetic energy (TKE) value is no longer imposed at model inlet: it adjusts itself with flow dynamics. Another advantage of the cyclic method is the reduced time needed to obtain flow equilibrium, which is considered in the section dealing with convergence time evaluation.

Initial and Boundary Conditions and Turbulence Model

Initial conditions corresponded to a static state with velocity vector $U = 0$ and water depth $H = 0.10$ m; this last value corresponds to the mean water height measurement by Tran et al. (2016) for a flowmeter value $Q = 0.05$ m^{3}s^{-1} with a flume tilted at slope $S = 5\%$. The bottom mesh was assumed to be as horizontal and the force of gravity was given by g components $g_x = 0.48989$ ms^{-2} and $g_z = -9.79776$ ms^{-2}. Concerning BCs, the principle of the cyclic mode was to apply at the inlet the variable values obtained at the outlet, which considerably simplified VOF simulation. Bot tom and cylinders walls were considered as smooth, and a classical wall law was used. Numerical tests showed that the dimensionless wall distance $y^+ = (u_* y)/v$ was $29 < y^+ < 341$ for the coarse mesh and $2 < y^+ < 345$ for the fine mesh. The weak values were very localized for the fine mesh, and the mean value of y^+ was about 90, so wall law application remained legitimate. For the flume lat eral walls, a no friction condition (symmetry) was applied, and it was verified in this case that a wall law applied to the side walls gave similar results. The choice of a turbulence closure model from the wide panel in the OpenFOAM library was not obvious and had to be validated by experimental comparison. Following the results by Ducrocq et al. (2017) with a single obstacle, the SSTk ω model was used for the two meshes, hereafter called KOM1 for the coarse mesh and KOM2 for the fine mesh. Simulation with Smagorinsky large eddy simulation was only used with the finer Mesh2.

The discharge value Q was the result of calculation, gradually increasing from zero to an equilibrium value, and we were able to verify that the obtained value fluctuated for all tested cases around $Q = 0.052$ 0.053 m^{3}s^{-1}, which is a good result relative to the uncertainty concerning the mean value of experimental water depth and demonstrates that the numerical model reproduced quite well the global friction effects and resistance forces exerted by obstacles.

Table 3. Time step values and CPU time cost to simulate 1 s for three tested models on one core of EOS supercomputer

Time specification	KOM1 (coarse)	KOM2 (fine)	LES (fine)
Time step (s)	2×10^{-3}	2.2×10^{-4}	2.5×10^{-4}
CPU time to simulate 1 s (h)	9	128	175

Note: CPU times for KOM2 and LES built upon fine mesh are of the same order of magnitude.

Convergence Time Evaluation

The necessary duration to reach a state of equilibrium of mean flow is critical, due to the very short time step required by the Courant Friedrichs Lewy (CFL) condition added to the constraints inherent to the VOF convergence method. The computations were made on the EOS supercomputer at the CALMIP Center at the Univ. of Toulouse, France because of the parallel capacities of OpenFOAM code. The CPU times were substantial; Table 3 lists the values of the time step and the CPU times for 1 processor (Intel Ivybridge 2.8 GHz) to simulate 1 s for the three tested models. Time steps were continuously adjusted by OpenFOAM solver in order to sat isfy a Courant number less than or equal to 1. Nevertheless, start ing from an initial state of rest, the first computation outputs showed that the simulated time necessary to obtain the established flow was surprisingly short compared with flume experiments and with calculations using classical BC simulations: after about 10 s, the discharge value converged around a mean value. Because of the cyclic mode, the flow was smoothly driven by gravity without having to sustain traveling waves caused by artificially forced boundary conditions.

In order to verify the necessary time to obtain an established flow, a simplified calculus was used, considering a control volume of fluid starting from rest and submitted to gravity and to a global drag force of obstacles. The comparison of the discharge calculated in this way with $Q(t)$ from OpenFOAM confirmed the order of magnitude of time to reach the state of equilibrium (Fig. 3). Never theless, a deeper analysis of the local values of velocity variables showed that the convergence process did not apply equally to all points (slower convergence for low velocity zones), and it was therefore deemed preferable to consider the results from at least a simulated time of 20 s.

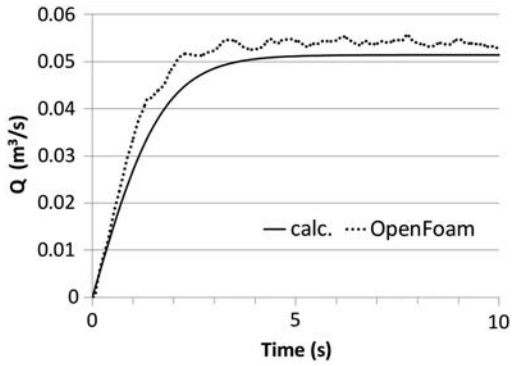

Fig. 3. Calculated and OpenFoam modeled evolution of the discharge versus time at the outlet from initial rest state. Only times shorter than 10 s are considered, but fully developed flow corresponds to about 20 s.

Model Validation

Water Depth

The interFoam solver uses a single field α to represent the phase percentage in a given cell: 0 corresponds to 100% air, and 1% 100% corresponds to water. The VOF method used in interFoam does not explicitly reconstruct the free surface, which is not crip pling in the present case. Due to the vertical thickness of the grid, locating the free surface at $\alpha = 0.5$ in cells provided sufficient pre cision (2 mm maximum). During the simulation, the mean water height remained at the initial height of 0.10 m due to good mass conservation. The value of the longitudinal bottom slope induced a relatively high Froude number (0.83) and a free surface with marked distortions around the obstacles and a strong level of ag itation. Results when using LES turbulence modeling [Fig. 4(b)] had this characteristic, whereas SST $k\,\omega$ [Fig. 4(a)] obtained a smoother free surface, which is usual with an URANS model. The average difference between the minimal and maximal values was about 0.025 m, and for some locations the difference was 0.06 m. Experimental flow observations confirmed the agitated as pect provided by the LES model. Mean water surface elevation was measured by an optical method (Cassan et al. 2014) and compared with calculated mean water depths along an axial section of ob stacles obtained respectively with SST $k\,\omega$ on coarse mesh (KOM1) and fine mesh (LES) (Fig. 5). The two calculated results correctly represent the mean free surface location, according to an

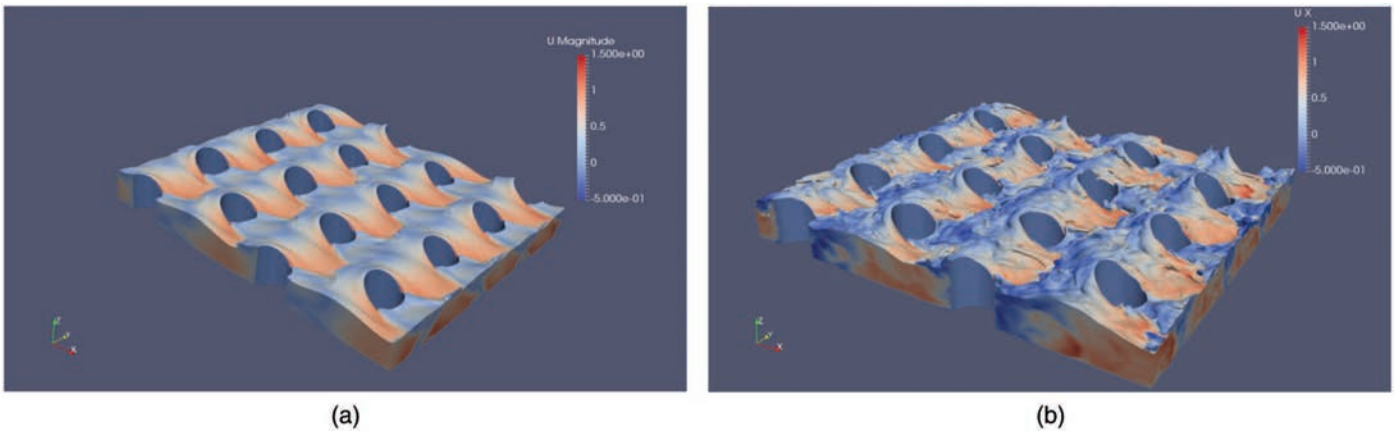

Fig. 4. (Color) Instantaneous free surface aspect obtained with finer mesh with (a) (KOM2); and (b) more realistic (LES). Color levels correspond to U component magnitude.

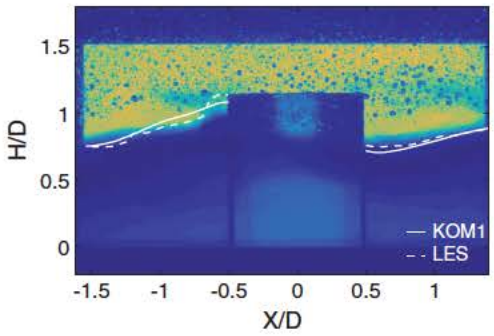

Fig. 5. (Color) Side view of experimental water surface profile along an obstacle axis obtained by data from Tran et al. (2016) and KOM1 and LES results ($C = 16\%$, $S = 5\%$, and $Q = 50$ L/s).

uncertainty of depth estimated at ±5 mm relative to optical measurements (Tran 2015).

Velocities

Comparison of the three velocity components (U, V, and W) with ADV measurements along Axial section 3 at plane $Z/h = 0.4$ (Fig. 6) showed that the two turbulence models provided good representation of the flow between obstacles. This contracted passage was characterized by a maximum U value approaching the V_g reference. On the other hand, the results in the wake showed that coarse mesh induced a significant error by overestimating U values. This fact is of particular importance for possible fish rest zones. Along this axial section, the V component value was close to zero. Longitudinal velocities departed from measurement values in the wake zone with coarse mesh. Vertical velocity W values were in accordance with flow description of Cassan et al. (2014) and Baki et al. (2014a). Upwelling velocities increased and decreased inversely with water depth. Their amplitude was relatively weak and always less than 10% of V_g. Hereafter, particular attention is paid to W parameter values because fish are sensitive to variations in vertical velocities (Liao 2007).

In order to verify the capacity of the simulation to correctly predict hydrodynamics in the wake zone, velocities along Transverse section 4 are given in Fig. 7. Values of the U component confirmed that using a coarse mesh led to significant error in obstacle axial minimum value. Maximal velocities, possibly greater than V_g, were encountered along the sides of obstacles. Transverse component V values were similar for the two models due to the flow constraint to pass the flow through the next interval between obstacles, and varied between ±30% of V_g. Vertical velocities W remained weak, less than 10% of V_g, but were well reproduced. However, flow upwelled along the axis of the obstacle wake ($Y/D = 1.2$), whereas it downwelled at the wake edges ($Y/D = 0.9$ 1.5). These velocity gradients induced a strong turbulence level (discussed in the following section), although the averaged velocity remained low.

Turbulent Kinetic Energy

For the SST k ω model, the turbulent kinetic energy $k(t)$ is given directly by the resolution of its transport equation. For LES simulation, $k(t)$ is calculated from instantaneous velocity values sampled at time steps of 0.01 s, and K corresponds to a value averaged over a 10 s period. Fig. 8 shows turbulent kinetic energy K profiles for Sections 3 5. LES model results better described K values, particularly in the wake zone where the K/V_g^2 value was about 10%. In the jet, K/V_g^2 was about 5%, showing that the turbulence level was not greater than that observed in a natural river (Nezu and Nakagawa 1993).

Spectral analysis of $k(t)$ revealed that the smallest scale fluctuations were resolved very differently depending on the turbulence model (Fig. 9). In accordance with Ostanek and Thole (2012), who studied the influence of streamwise spacing in an array of staggered

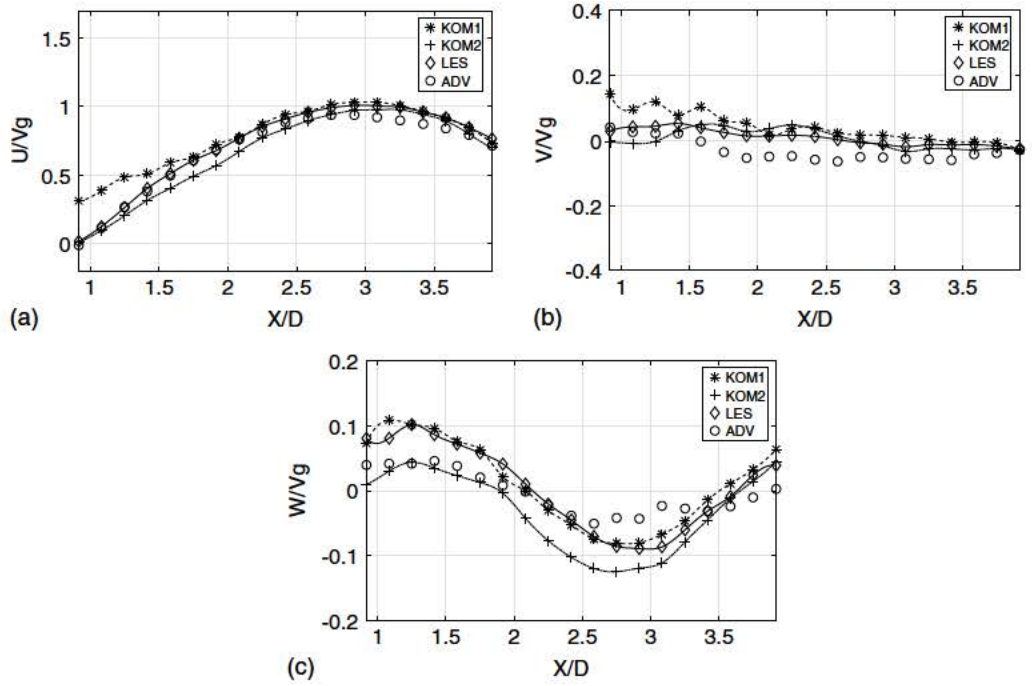

Fig. 6. Velocity components along Section S3 at plane $Z/h = 0.4$ obtained by models and ADV measurements from Tran et al. (2016): (a) U; (b) V; and (c) W. Numerical results are averaged over 30 s.

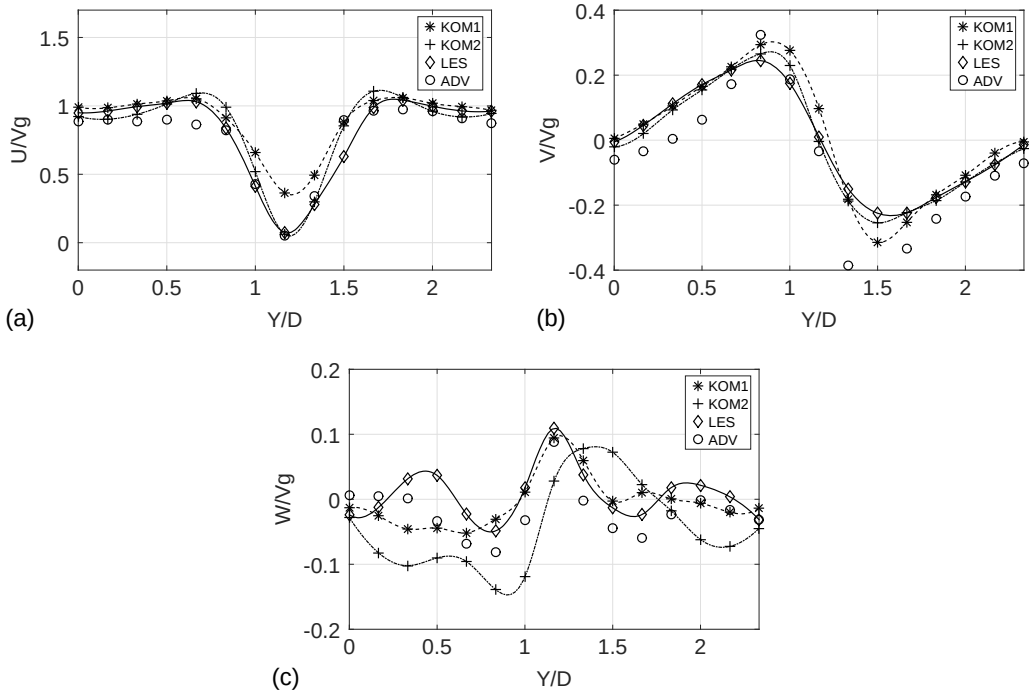

Fig. 7. Velocity components along Section S4 at plane $Z/h = 0.4$ obtained by models and ADV measurements from Tran et al. (2016): (a) U; (b) V; and (c) W. Numerical results are averaged over 30 s.

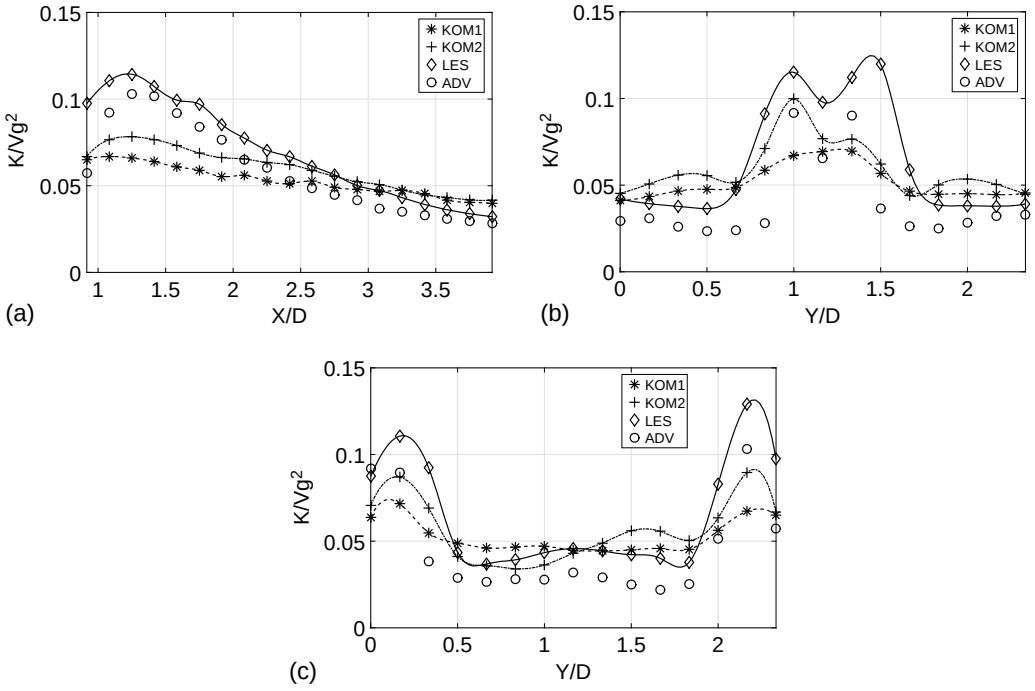

Fig. 8. Turbulent kinetic energy profiles obtained by models and ADV measurements from Tran et al. (2016) along (a) Section S3; (b) Section S4; and (c) Section S5. Numerical results are averaged over 30 s.

cylinders, we assumed that a slope of $-5/3$ for the $k(t)$ spectrum means a good representation of the turbulence. As expected, the coarse mesh did allow calculating fluctuations for $St < 1$. With the fine mesh, the smallest scale fluctuations were detected beyond $St = 1$, allowing a better description of possible fish rest zones. With the LES model, a wide bandwidth of inertial spectrum was well resolved, which is proof of accurate modeling. The LES model reproduced the spectral peak for $k(t)$ measured along the mixing zone at the wake edges, which was not revealed by SST $k\,\omega$ models.

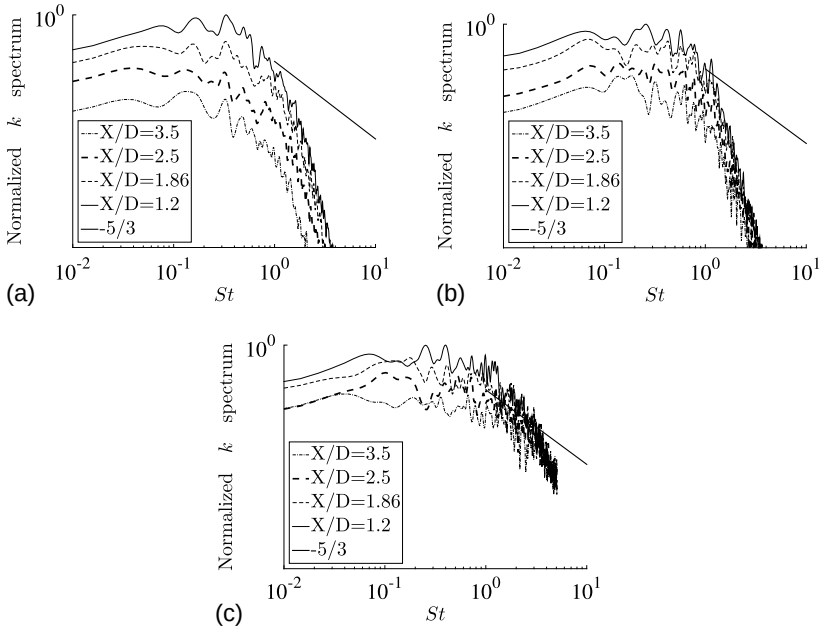

Fig. 9. Spectrum of turbulent kinetic energy as a function of the Strouhal number at Section S3 for various X/D: (a) KOM1; (b) KOM2; and (c) LES.

Discussion for Fish Passability

Design Criteria for Rock-Ramp Fishways

In the contracted flow zone between the obstacles, U values can be prohibitive if they are incompatible with fish species. The charac teristics for rock ramp fishways must take into account compatible fish swimming capacities and the existence of rest zones located in obstacle wakes: adverse longitudinal U velocities, W vertical inten sities, turbulent kinetic energy K level, and lateral V oscillation fre quency. Concerning adverse U velocities in the wakes, Cabonce et al. (2018) and Cabonce et al. (2017) observed that juvenile silver perch became lost and faced downstream in the wakes of baffles and were often unable to pass the obstacle. Particular attention must be paid to W values because fish are sensitive to variations in ver tical velocity (Liao 2007). It is difficult to predict the behavior of a fish exposed to velocity fluctuations, depending on species and size of the animal (Odeh et al. 2002; Liao 2007; Tritico and Cotel 2010; Cote and Webb 2015). Usual fishway design rules are based upon the limitation of mean dissipated hydraulic power, and therefore neglect local flow characteristics and their temporal fluctuations. Nevertheless, the choice of a fish friendly configuration can depend upon criteria such as potential rest zone area (Tran et al. 2016), maximal admissible velocity, and turbulence level. By analogy with vertical slot fishways, e.g., Calluaud et al. (2015), who tested chubs of 9.7 15.9 cm total length, an efficient rest zone should satisfy $U < 0.3$ ms ^{1} and $K < 0.4$ m^{2}s ^{2}. Qualitative flow features may be determinant relative to ramp efficiency, and experiments by Tritico and Cotel (2010) showed the importance of eddies spinning around a horizontal axis in perturbing the stability of creek chubs. The turbulent kinetic energy K was shown by Enders et al. (2005) to increase swimming costs for juvenile Atlantic salmon. Silva et al. (2012) observed that turbulent variables influenced the swimming behavior in an experimental pool type fishway of small fish, which could not hold position and dropped back to the adjacent down stream pool. Silva et al. stated that the most influential turbulent parameter for fish behavior of both size classes in their experi ments was the Reynolds shear stress, which affects fish swimming performance and stability. Another flow feature determinant for fish behavior observed by Silva et al. was eddy size, a parameter which is difficult to determine from the velocity field. Small fish facing eddies larger than their size generally swam through eddies with larger lateral body amplitudes and curvatures and were rarely disoriented, normally successfully ascending the fishway (Silva et al. 2012).

Relevance of CFD Results to Fish Passage

Velocities

The KOM1 model demonstrated that with very much shorter CPU times than LES, a relatively coarse mesh associated with an appro priate URANS turbulence model to treat separated flow such as SST $k\ \omega$ can reproduce mean adverse velocities that prevent fish swimming upstream (Baki et al. 2017). The absolute velocity, re lated to species dependant fish criteria (Mateus et al. 2008), can be deduced from the dimensionless velocity in Figs. 6 and 7. The KOM1 model can also be used to assess the energy spent by fish, which is proportional to the cube of local velocity (Wang and Chanson 2018). Nevertheless, severe limitations of this modeling were encountered in the wake zone, principally due to weak mesh density, and KOM1 induced a significant error by overestimating U values. This is of particular importance for the position of a resting area for the fish. Using a fine mesh with the SST $k\ \omega$ model (KOM2) improved the precision in these zones, but this model does not offer a worthwhile CPU time:quality ratio compared with LES (Table 3). The general flow structure obtained with KOM1 and LES models is illustrated in Fig. 10 by instantaneous velocity profiles shown on two horizontal slices located at $Z/h = 0.4$ and 0.7. Blank zones visible on plane $Z/h = 0.7$ correspond to local air inclusions, a diphasic feature which was observed in an experimental flume for this configuration. Nonstationary wakes appeared in both models, but, as expected with LES, smaller structures were observed, a valu able capacity for estimating fish adaptation to hydrodynamics. The strongest velocity amplitudes were encountered along the sides of obstacles, irrespective of Z elevation above the bottom.

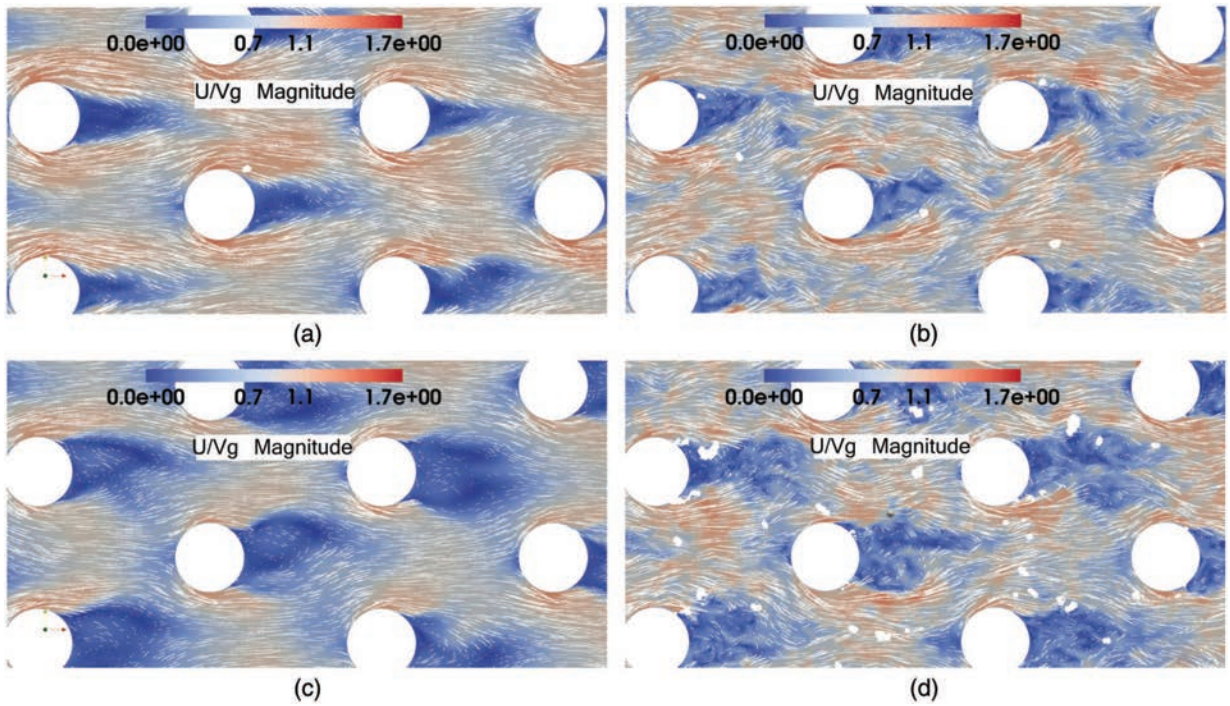

Fig. 10. (Color) Velocity vector maps: (a) KOM1 at plane $Z/h = 0.4$; (b) LES at plane $Z/h = 0.4$; (c) KOM1 at plane $Z/h = 0.7$; and (d) LES at plane $Z/h = 0.7$.

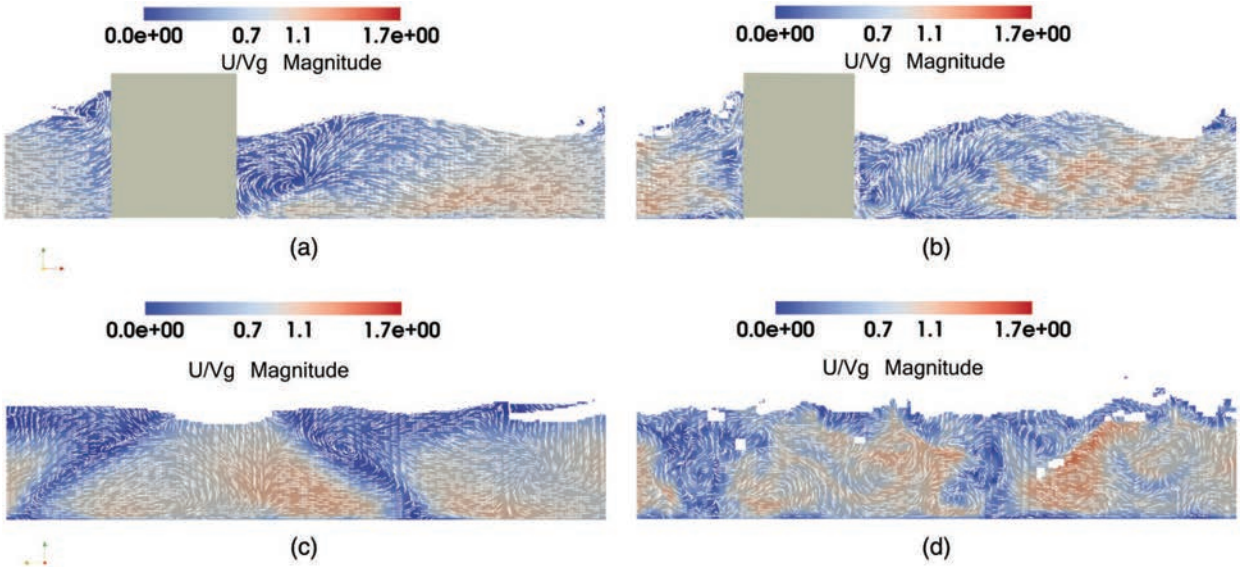

Fig. 11. (Color) Velocity vector maps: (a) KOM1 at longitudinal obstacle centered plane; (b) LES at longitudinal obstacle centered plane; (c) KOM1 at transverse plane $X/D = 1.4$; and (d) LES at transverse plane $X/D = 1.4$.

Lateral expansion of the wake was wider near the free surface due to oscillatory movements with a larger amplitude. Vertical slices in Fig. 11 confirm this observation. Moreover, it appears that, although velocity magnitudes were similar in the two models, flow structure itself was quite different. For the KOM1 model, a single, wide vertical structure is visible in the wake, whereas for the LES model smaller structures were detected ($\cong D/3$), which is a significant feature for fishway design. The illustration corresponds to an instantaneous time step, but the preceding observations apply to all obstacle wakes at any time step. The conclusions relative to a single obstacle exposed to a Froude number with the same order of magnitude as that given by Ducrocq et al. (2017) are reliable. Although near the free surface the weak velocity zone has an order of magnitude D, this zone is reduced near the bottom and therefore does not provide a convenient resting place for fish.

Fluctuations

For lateral $v(t)$ fluctuations, LES appears capable of reproducing the vortex street shedding which conditions fish Karman gaiting attitude (Liao et al. 2003). In this case, fish can synchronize their

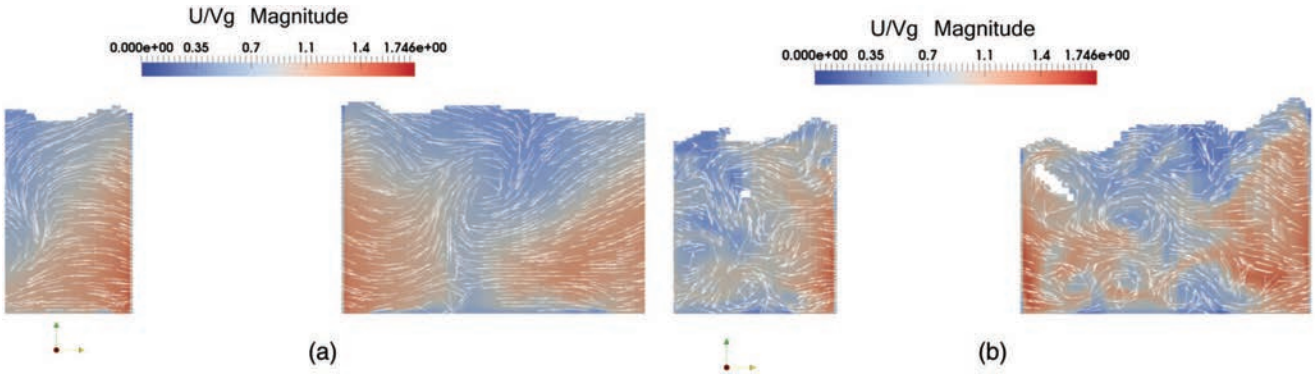

Fig. 12. (Color) Velocity vector map at Transverse section 2 (minimum distance between two blocks): (a) KOM1; and (b) LES.

body motions with the vortex shedding frequency and adopt a lower tail beat frequency and larger lateral body curvature, neces sitating less energy expenditure. The strength of the LES model is its capacity to reproduce unsteady flow including small structures ($St > 1$), as shown in the preceding section. This is a significant feature in the design of fishways suitable for small fish species such as cyprinids (Santos et al. 2012), which are predominant in rivers. In Fig. 12, velocity vectors show that strong instantaneous vertical and transverse velocities can be encountered in the zones between obstacles, which are favorable to fish passage. The magnitude of these fluctuations can be deduced from k, but it is more difficult to predict their size.

It was previously shown from a comparison of kinetic turbulent energy spectra $k(t)$ that LES can detect finer flow structures than can SST $k\ \omega$, which is a well known result but of primary impor tance for a fine prediction of fish response. In order to estimate unsteady movements relative to fish behavior, the spectra of lateral $v(t)$ velocity fluctuations are illustrated in Fig. 13, showing that the Strouhal number $St = 0.17\ \ 0.18$ is enhanced with both the coarse and fine mesh patterns using the SST $k\ \omega$ model. For obstacle ar rangements, the frequency of these vortices does not differ signifi cantly from 0.2 (Ghomeshi et al. 2007), although a slightly larger value might have been expected (Ziada 2006). For the k spectrum, the finer mesh KOM2 model requires that more structures are re solved, and a second peak appears in the spectrum which can be related to the bed and other obstacle interaction.

With the LES model, the same frequency appears but it is capable of dealing with a better resolution of complex structures induced by surrounding obstacles. The maximum peak was en countered for $St = 0.24$, which is better suited to experimental value (Ghomeshi et al. 2007; Ziada 2006) for flows with a high Reynolds number. This Strouhal value is located at the lower bound of the interval $0.25 < St < 0.35$, corresponding to the maximum propulsive efficiency for aquatic animals given by Eloy (2012) cit ing Triantafyllou et al. (1993). Other peaks were similar for the KOM2 model, which shows that the KOM1 model appears to be able to realistically reproduce the more energetic oscillations ($St \approx 0.2$). Nevertheless, the mean velocities may be overestimated

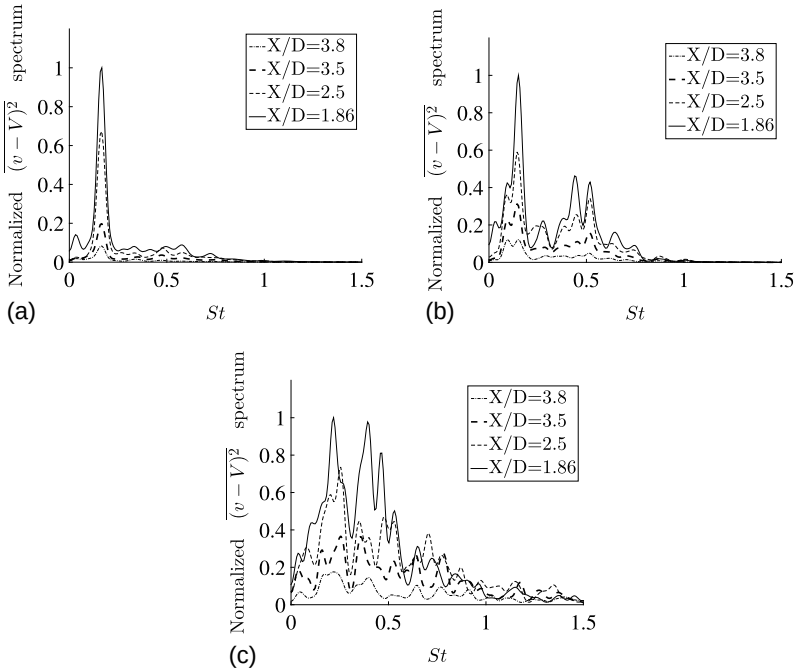

Fig. 13. Spectrum of the transverse fluctuations as a function of the Strouhal number at Section S3 for various X/D: (a) KOM1; (b) KOM2; and (c) LES.

(Fig. 7) due to an underestimated turbulent kinetic energy K (Fig. 8). KOM2, with its finer mesh, can decrease this gap, but the LES model remains the most pertinent for satisfactory turbulence modeling in flows with separation zones. KOM2 has a CPU time similar to that of LES (Table 3), and consequently, only the capacities of the KOM1 and LES models are hereafter examined.

Flow Features

The streamlines in Fig. 14 clearly show upwelling velocities in the wake at a distance of about $X/D = 1.5$ associated with a rotative movement around a downward oriented axis. Similar wakes structures were found in numerical modeling by Baranya et al. (2012) although the weaker Froude numbers induced quasi vertical axes. Kirkil and Constantinescu (2015) found a similar shape of the wake even with weak Froude numbers. The LES model results distinctly reproduced the horseshoe vortex structure at the bottom of the obstacles using the standard Q criterion, $Q > 0$, demonstrating the balance between vorticity magnitude and deformation strain rate (Fig. 15). The threshold used for picture readability is $Q > 500$, clearly showing the locations of horseshoe vortex zones around the bases of obstacles and other potential eddy regions. A significant difference between KOM1 and LES is that the horseshoe vortex structure at the bottom of the obstacles appears more clearly in LES simulation. This emphasizes that the LES model better represents the flow in the near bottom zone, which can be significant because fish passage is often observed in this zone (Santos et al. 2012).

The previous validation and model comparison indicate that fine numerical modeling can satisfactorily reproduce not only the mean velocity field but also the unsteady flow properties. As a consequence, we discuss how these models can provide information to aid fish pass design. Knowing the turbulent intensity and the Strouhal number at a large scale will provide the fluctuations for a given configuration (C, D, h, S, and Q). The flow compatibility can be assessed as a function of the fish species. The discussion deals with the best numerical procedure to use If the

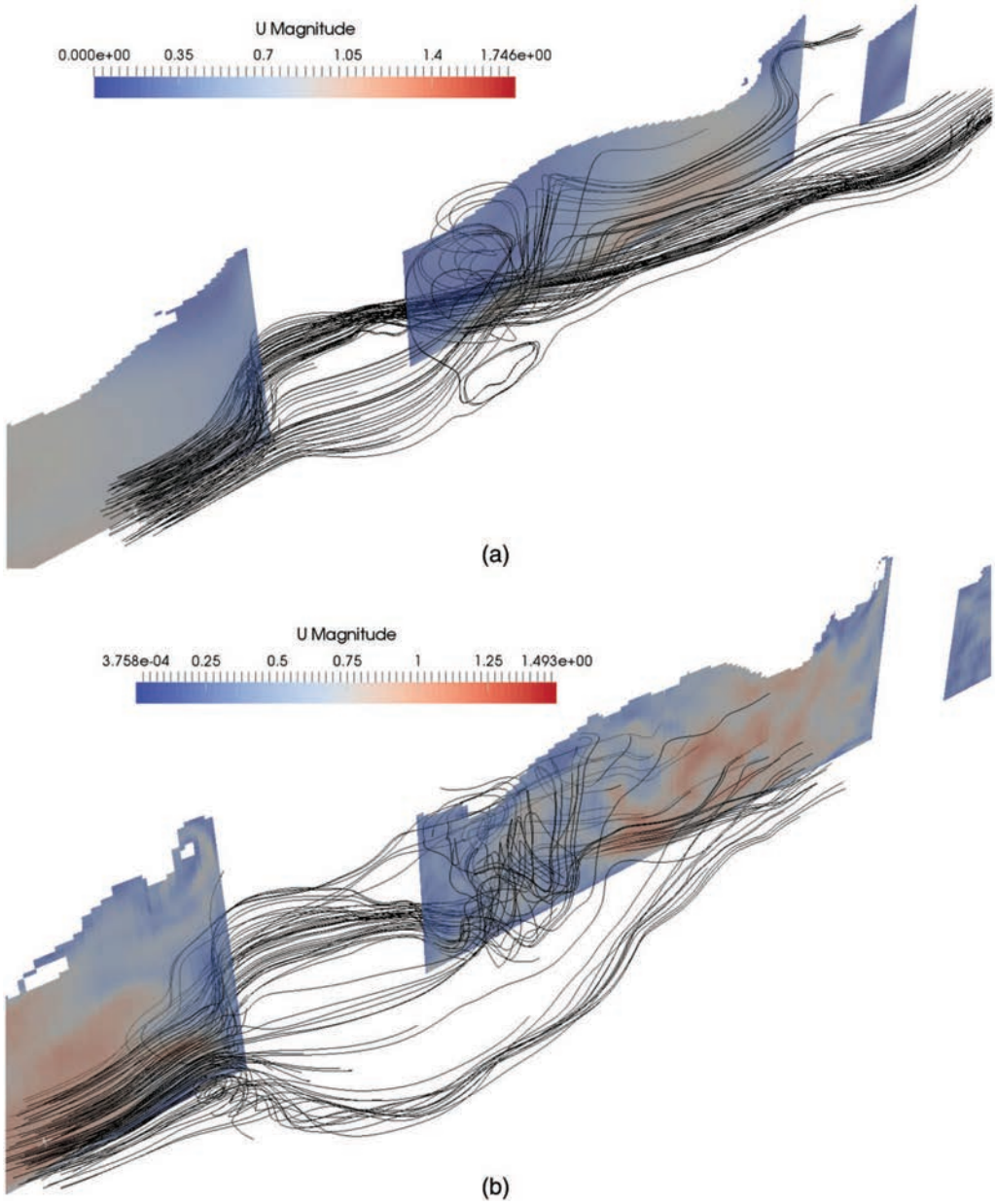

Fig. 14. (Color) Streamlines and longitudinal centered section around an obstacle: (a) KOM1; and (b) LES.

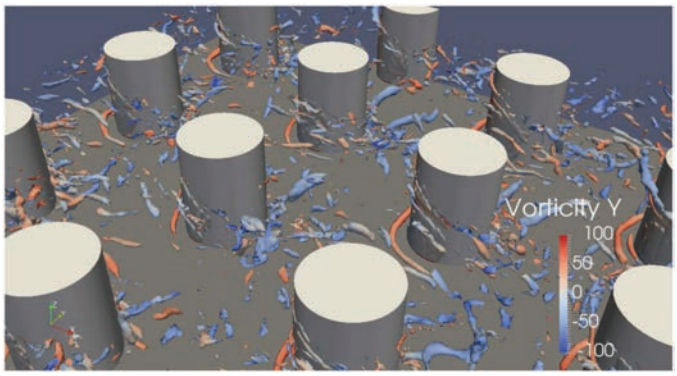

Fig. 15. (Color) LES model view of the isovorticity zones revealed by Q criterion $Q > 500$. Colored zones represent the vorticity value.

geometric configuration differs greatly from the one tested. An advantage of the LES model is its ability to reproduce large scale flow structures (order of magnitude D) which are comparable to fish size and liable to impede upstream migration. They are likely to impede upstream fish migration. The LES model provides better knowledge of free surface flow hydrodynamics through this steep slope arrangement of obstacles.

Full-Scale LES Model

To test the applicability of LES results to a larger geometrical scale corresponding to a real fishway and the possible influence of the Reynolds number on the results, the numerical model geometry was multiplied by $\lambda = 4$; therefore the initial water depth $h_0 = 0.10 \times 4 = 0.40$ m through obstacles of $D = 0.115 \times 4 = 0.46$ m. The resulting flow discharge value obtained at fully developed flow was about 1.6 $m^3 s^{-1}$, otherwise satisfying the Froude similarity discharge scale $\lambda^{5/2} = 32$. Froude similarity applies for flow around obstacles as long as energy dissipation is principally due to drag forces and near bottom flow remains fully rough (Cassan et al. 2014). In our simulation, the flume bottom was smooth but results were very close for the two tested scales with a Reynolds ratio of 8 (Fig. 16).

Data obtained by Calluaud et al. (2015) gave $U < 0.3$ ms $^{-1}$ and $K < 0.4$ $m^2 s^{-2}$ for chubs. At prototype scale, $V_g = 1.66$ ms $^{-1}$ gives $(U/V_g)_{max} = 0.18$ and $(k/V_g^2)_{max} = 0.14$. In Fig. 16 along obstacle axis at $Z = 0.16$ m from the bottom, the limit is located at about $X/D = 1.2$, giving a distance of $0.7D = 0.34$ m behind the obstacle. Concerning lateral fluctuations, the $v(t)$ spectrum shows that the same frequency as that of the scale model was found (Fig. 17), and confirms that the value $St = 0.2$ provides a good estimation of the velocity fluctuations. Santos et al. (2012) stated that Reynolds shear stress (RSS) intensity was one of the factors that most influenced fish movements. At two locations $X/D = 1.2$ (behind the obstacle) and $X/D = -0.84$ (in front of the obstacle), Table 4 gives the mean values of velocities (U, V, and W) and the median absolute value for the three RSS components ($\rho|u'v'|$, $\rho|u'w'|$, and $\rho|v'w'|$). At $X/D = 1.2$, the median vertical stress $\rho|u'w'| = 69$ Nm $^{-2}$ has the same order of magnitude as that found in natural streams during a flash flood (Odeh et al. 2002). Consequently, the alleged rest zone does not appear as an ideal fish friendly location. It must be taken into account that the slope $S = 5\%$ and

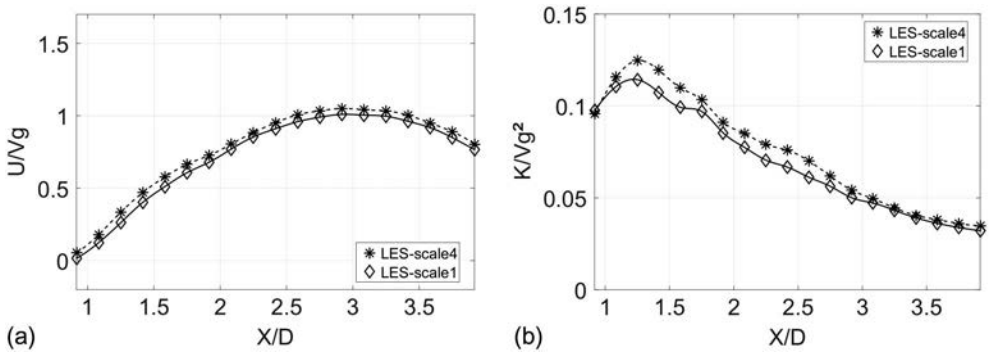

Fig. 16. Evaluation of scale effect at Section S3 using LES model: (a) velocity component U; and (b) kinetic turbulent energy K. Scale 4 represents the simulation with a prototype fish pass (Reynolds = 796,800); Scale 1 the simulation at experimental setup scale used by Tran et al. (2016) (Reynolds = 99,600).

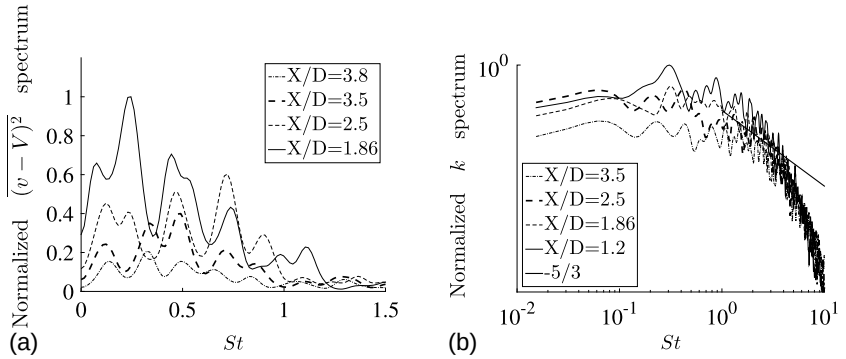

Fig. 17. Spectra as a function of the Strouhal number at prototype scale along Section S3 in LES model: (a) $v(t)$; and (b) $k(t)$.

Table 4. Values of U, V, and W and median RSS absolute values behind and in front of the obstacle at X/D 1.2 and 0.84, at Z 0.16 m

X/D	U (m/s)	V (m/s)	W (m/s)	$\rho\lvert u'v'\rvert$ (N/m^2)	$\rho\lvert u'w'\rvert$ (N/m^2)	$\rho\lvert v'w'\rvert$ (N/m^2)
1.2	0.480	0.014	0.255	86	69	92
0.84	1.30	0.07	0.11	27	30	26

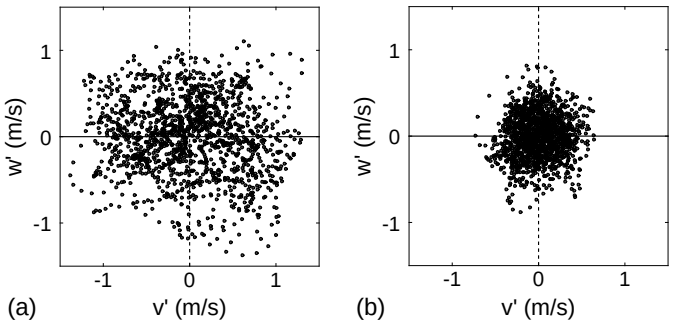

Fig. 18. v' w' fluctuations at prototype scale at $Z = 0.16$ m: (a) behind the obstacle at $X/D = 1.2$ and $U = 0.48$ m/s; and (b) in front of the obstacle at $X/D = 0.84$ and $U = 1.3$ m/s. Data sampled at 100 Hz for 15 s.

Froude $Fr = 0.83$, values chosen to test the models' capabilities, correspond to a harsh configuration for small fish. In contrast with the downstream probe, the probe located at $X/D = -0.84$ in front of the obstacle was subjected to a mean longitudinal velocity $U =$ 1.30 m/s but the fluctuations and RSS were much weaker. The transverse versus vertical fluctuations observed behind an obstacle at $X/D = 1.2$ and -0.84 are given in Fig. 18, showing that v' and w' amplitudes can exceed 1 ms ^{1} at $X/D = 1.2$; such events are able to sweep or eject fish from the wake, in contrast with weaker fluctuations in front of the obstacle. Therefore, if fish can withstand the U value they can remain in a quasi stationary position immedi ately upstream of the obstacle, as observed by Cabonce et al. (2018) with juvenile silver perch. This observation confirms that a fine knowledge of fluctuations in such complex flows is necessary in order to ensure that conditions are suitable for fish, which will have to be validated by laboratory and in situ tests with fish.

Conclusion

The main purpose of this work was to advance fine numerical mod eling of complex free surface flows around staggered and unsub merged cylinders, because flows are of great importance to ensure upstream passage of fish. Nature like fishways work well for strong swimming fish such as salmonids, but are rarely accessible for small species such as cyprinids. To improve access for the latter, we need a better and finer knowledge of such complex flows. Due to the geometrical periodicity, we were able to use the open source code OpenFOAM by adapting cyclic boundary conditions. This method, which is rarely used for free surface flow modeling, en abled us to avoid the prescription of artificial boundary conditions, to reduce the modeled length, and to provide a progressive accel eration of flow with gravity force. The reduction of CPU time by using cyclic BCs allowed us to run LES on a fine mesh. The chosen test case, with a longitudinal slope of 5% and concentration of ob stacles $C = 16\%$, corresponding to an upper limit ramp for such natural fishways, was validated by experimental measurements. Two models were retained: KOM1 (coarse mesh, SST k ω) and LES (fine mesh, Smagorinsky LES). KOM1 gives more than acceptable results except in the vicinity of obstacles and for turbu lent kinetic energy (TKE) values. It can also calculate fluctuations for $St < 1$. Such a model can be used profitably during the design phase of an engineering project necessitating numerous optimiza tion tests. On the other hand, as expected, the LES model gives the best results, especially in the wake zones corresponding to possible fish rest or Karman gait behavior. On a candidate fish pass configu ration, the model's high resolution can be used in particular to ex plore transient fluctuations in the wakes of obstacles. Nevertheless, its CPU cost, despite cyclic BCs, remains rather prohibitive for testing multiple configurations and optimizing the arrangement of obstacles. In this study, tests were made with a smooth bottom for validation considerations, but such fish passes are generally covered with pebbles. Further modeling should include the effect of bottom roughness, and the dynamic rough wall law used by Uchida et al. (2016) in the case of submerged staggered boulders may be an interesting alternative to a prescription involving the simplest roughness height. A new large glass walled tilted flume was installed at IMFT in spring of 2018, and experiments on real fish behavior in such flows have already begun.

Acknowledgments

The calculations were performed on the EOS supercomputer at CALMIP, Toulouse, France, which is gratefully acknowledged.

Notation

The following symbols are used in this paper:

a_X = longitudinal distance between obstacles (m);
a_Y = transverse distance between obstacles (m);
B = flume width (m);
C = obstacle concentration;
D = diameter of cylinders (m);
f = fluctuation frequency (Hz);
g = gravity acceleration (ms ^{2});
h = water depth (m);
K = time averaged turbulent kinetic energy (m^{2}s ^{2});
k = turbulent kinetic energy (m^{2}s ^{2});
p = pressure (Nm ^{2});
Q = water discharge (m^{3}s ^{1});
S = longitudinal flume slope;
St = Strouhal number based upon V_g;
t = time (s);
U = time averaged longitudinal velocity (ms ^{1});
U_c = critical swimming speed of fish (ms ^{1});
V = time averaged transversal velocity (ms ^{1});
V_g = velocity between obstacles (ms ^{1});
V_0 = bulk velocity (ms ^{1});
v = lateral velocity component (ms ^{1});
W = time averaged vertical velocity (ms ^{1});
X = longitudinal axis coordinate (m);

Y = transversal axis coordinate (m);
Z = vertical axis coordinate (m);
α = phase percentage air/water;
λ = geometric scale; and
ρ = volumetric water mass (kg · m ^{3}).

References

Baki, A., W. Zhang, D. Zhu, and N. Rajaratnam. 2014a. "Mean flow characteristics in a rock ramp type fish pass." *J. Hydraul. Eng.* 140 (2): 156 168. https://doi.org/10.1061/(ASCE)HY.1943 7900.0000816.

Baki, A., W. Zhang, D. Zhu, and N. Rajaratnam. 2014b. "Turbulence characteristics in a rock ramp type fish pass." *J. Hydraul. Eng.* 141 (2): 04014075. https://doi.org/10.1061/(ASCE)HY.1943 7900.0000962.

Baki, A., W. Zhang, D. Zhu, and N. Rajaratnam. 2016. "Flow simulation in a rock ramp fish pass." *J. Hydraul. Eng.* 142 (10): 04016031. https://doi.org/10.1061/(ASCE)HY.1943 7900.0001166.

Baki, A., W. Zhang, D. Zhu, and N. Rajaratnam. 2017. "Flow structures in the vicinity of a submerged boulder within a boulder array." *J. Hydraul. Eng.* 143 (5): 04016104. https://doi.org/10.1061/(ASCE)HY.1943 7900.0001273.

Baranya, S., N. R. B. Olsen, T. Stoesser, and T. Sturm. 2012. "Three dimensional rans modeling of flow around circular piers using nested grids." *Eng. Appl. Comput. Fluid Mech.* 6 (4): 648 662. https://doi.org/10.1080/19942060.2012.11015449.

Bretón, F., A. B. M. Baki, O. Link, D. Z. Zhu, and N. Rajaratnam. 2013. "Flow in nature like fishway and its relation to fish behaviour." *Can. J. Civ. Eng.* 40 (6): 567 573. https://doi.org/10.1139/cjce 2012 0311.

Cabonce, J., R. Fernando, H. Wang, and H. Chanson. 2017. "Culvert baffles to facilitate upstream fish passage." In *Proc., 13th Hydraulics in Water Engineering Conf. HIWE201*. Sydney, Australia: Engineers Australia.

Cabonce, J., H. Wang, and H. Chanson. 2018. "Ventilated corner baffles to assist upstream passage of small bodied fish in box culverts." *J. Irrig. Drain. Eng.* 144 (8): 0418020. https://doi/10.1061/%28ASCE%29IR .1943 4774.0001329.

Calluaud, D., V. Cornu, P. Baran, and L. David. 2015. "Relationship between fish behavior turbulence and unsteady flow in experimental vertical slot fishways." In *Proc., Int. Conf. on River Connectivity Best Practices and Innovations, Fish Passage 2015*. Karlstad, Sweden: North American Fish Passage Organisation, Karlstad Univ.

Cassan, L., T. Tien, D. Courret, P. Laurens, and D. Dartus. 2014. "Hydraulic resistance of emergent macroroughness at large Froude numbers: Design of nature like fishpasses." *J. Hydraul. Eng.* 140 (9): 04014043. https://doi.org/10.1061/(ASCE)HY.1943 7900.0000910.

Chanson, H., M. Trevethan, and C. Koch. 2007. "Discussion of 'turbulence measurements with acoustic doppler velocimeters' by Carlos M. García, Mariano I. Cantero, Yarko Nino, and Marcelo H. García." *J. Hydraul. Eng.* 133 (11): 1283 1286. https://doi.org/10.1061/(ASCE)0733 9429 (2007)133:11(1283).

Cote, A. J., and P. W. Webb. 2015. "Living in a turbulent world A new conceptual framework for the interactions of fish and eddies." *Integr. Comp. Biol.* 55 (4): 662 672. https://doi.org/10.1093/icb/icv085.

Ducrocq, T. 2016. "Etude de l'ecoulement à forte pente autour d'un cylindre émergent." Ph.D. thesis, Institute of Fluid Mechanics, Université de Toulouse.

Ducrocq, T., L. Cassan, J. Chorda, and H. Roux. 2017. "Flow and drag force around a free surface piercing cylinder for environmental applications." *Environ. Fluid Mech.* 17 (4): 629 645. https://doi.org/10.1007 /s10652 016 9505 9.

Eloy, C. 2012. "Optimal Strouhal number for swimming animals." *J. Fluids Struct.* 30 (Apr): 205 218. https://doi.org/10.1016/j.jfluidstructs.2012 .02.008.

Enders, E. C., T. Buffin Bélanger, D. Boisclair, and A. G. Roy. 2005. "The feeding behaviour of juvenile Atlantic salmon in relation to turbulent flow." *J. Fish Biol.* 66 (1): 242 253. https://doi.org/10.1111/j.0022 1112.2005.00599.x.

Ghomeshi, M., S. A. Mortazavi Dorcheh, and R. Falconer. 2007. "Amplitude of wave formation by vortex shedding in open channels." *J. Appl. Sci.* 7 (24): 3927 3934. https://doi.org/10.3923/jas.2007.3927.3934.

Graf, W., and I. Istiarto. 2010. "Flow pattern in the scour hole around a cylinder." *J. Hydraul. Res.* 40 (1): 13 20. https://doi.org/10.1080 /00221680209499869.

Hervouet, J. M. 2007. *Hydrodynamics of free surface flows: Modelling with the finite element method.* New York: Wiley.

Hinterberger, C., J. Froehlich, and W. Rodi. 2007. "Three dimensional and depth averaged large eddy simulations of some shallow water flows." *J. Hydraul. Eng.* 133 (8): 857 872. https://doi.org/10.1061/(ASCE) 0733 9429(2007)133:8(857).

Kawamura, T., S. Mayer, A. Garapon, and L. Sörensen. 2002. "Large eddy simulation of a flow past a free surface piercing circular cylinder." *J. Fluids Eng.* 124 (1): 91 101. https://doi.org/10.1115/1.14 31545.

Kirkil, G., and G. Constantinescu. 2015. "Effects of cylinder Reynolds number on the turbulent horseshoe vortex system and near wake of a surface mounted circular cylinder." *Phys. Fluids* 27 (7): 1070 6631. https://doi.org/10.1063/1.4923063.

Kirkil, G., S. G. Constantinescu, and R. Ettema. 2008. "Coherent structures in the flow field around a circular cylinder with scour hole." *J. Hydraul. Eng.* 134 (5): 572 587. https://doi.org/10.1061/(ASCE)0733 9429 (2008)134:5(572).

Lai, Y. G., L. J. Weber, and V. C. Patel. 2003. "Nonhydrostatic three dimensional model for hydraulic flow simulation. I: Formulation and verification." *J. Hydraul. Eng.* 129 (3): 196 205. https://doi.org/10 .1061/(ASCE)0733 9429(2003)129:3(196).

Liao, J. C. 2007. "A review of fish swimming mechanics and behaviour in altered flows." *Philos. Trans. R. Soc. London, Ser. B* 362 (1487): 1973 1993. https://doi.org/10.1098/rstb.2007.2082.

Liao, J. C., D. N. Beal, G. V. Lauder, and M. S. Triantafyllou. 2003. "The Kármán gait: Novel body kinematics of rainbow trout swimming in a vortex street." *J. Exp. Biol.* 206 (6): 1059 1073. https://doi.org/10.1242 /jeb.00209.

Liu, M., D. Z. Zhu, and N. Rajaratnam. 2002. "Evaluation of ADV measurements in bubbly two phase flows." In *Proc., Conf. on Hydraulic Measurements and Experimental Methods*, 10. Estes Park, CO: ASCE EWRI & IAHR.

Mateus, C. S., B. R. Quintella, and P. R. Almeida. 2008. "The critical swimming speed of Iberian barbel barbus bocagei in relation to size and sex." *J. Fish Biol.* 73 (7): 1783 1789. https://doi.org/10.1111/j.1095 8649 .2008.02023.x.

Menter, F. R. 1994. "Two equation eddy viscosity turbulence models for engineering applications." *AIAA J.* 32 (8): 1598 1605. https://doi.org /10.2514/3.12149.

Menter, F. R., M. Kuntz, and R. Langtry. 2003. "Ten years of industrial experience with the SST turbulence model." In *Proc., 4th Int. Symp. on Turbulence, Heat and Mass Transfer.* New York: Begell House.

Nepf, H. M., J. A. Sullivan, and R. A. Zavistoski. 1997. "A model for diffusion within emergent vegetation." *Am. Soc. Limnol. Oceanogr.* 42 (8): 1735 1745. https://doi.org/10.4319/lo.1997.42.8.1735.

Nezu, I., and H. Nakagawa. 1993. *Turbulence in open channel flows: IAHR monograph*. Rotterdam, Netherlands: A.A. Balkema.

Odeh, M., J. Noreika, A. Haro, A. Maynard, T. Castro Santos, and G. Cada. 2002. *Evaluation of the effects of turbulence on the behaviour of migratory fish*. Rep. No. DOE/BP 00000022 1. Portland, OR: Bonneville Power Administration.

Ostanek, J. K., and K. A. Thole. 2012. "Wake development in staggered short cylinder arrays within a channel." *Exp. Fluids* 53 (3): 673 697. https://doi.org/10.1007/s00348 012 1313 5.

Santos, J. M., A. Silva, C. Katopodis, P. Pinheiro, A. Pinheiro, J. Bochechas, and M. T. Ferreira. 2012. "Ecohydraulics of pool type fish ways: Getting past the barriers." *Ecol. Eng.* 48 (Nov): 38 50. https://doi.org/10.1016/j.ecoleng.2011.03.006.

Shao, W. Y., Y. P. Zhang, D. Z. Zhu, and T. Q. Zhang. 2013. "Drag force on a free surface piercing yawed circular cylinder in steady flow." *J. Fluids Struct.* 43 (Nov): 145 163. https://doi.org/10.1016/j.jfluidstructs.2013.09.007.

Silva, A. T., C. Katopodis, J. M. Santos, M. T. Ferreira, and A. N. Pinheiro. 2012. "Cyprinid swimming behaviour in response to turbulent flow." *Ecol. Eng.* 44 (Jul): 314 328. https://doi.org/10.1016/j.ecoleng.2012.04.015.

Tran, T. D. 2015. "Métrologie et modélisation des écoulements à forte pente autour d'obstacles: Application au dimensionnement des passes nature lles." Ph.D. thesis, Institut de Mécanique des Fluides de Toulouse, Université de Toulouse.

Tran, T. D., J. Chorda, P. Laurens, and L. Cassan. 2016. "Modelling nature like fishway flow around unsubmerged obstacles using a 2D shallow water model." *Environ. Fluid Mech.* 16 (2): 413 428. https://doi.org/10.1007/s10652 015 9430 3.

Triantafyllou, G. S., M. S. Triantafyllou, and M. A. Grosenbaugh. 1993. "Optimal thrust development in oscillating foils with application to fish propulsion." *J. Fluids Struct.* 7 (2): 205 224. https://doi.org/10.1006/jfls.1993.1012.

Tritico, H. M., and A. J. Cotel. 2010. "The effects of turbulent eddies on the stability and critical swimming speed of creek chub." *J. Exp. Biol.* 213 (13): 2284 2293. https://doi.org/10.1242/jeb.041806.

Tseng, M. H., C. L. Yen, and C. C. S. Song. 2000. "Computation of three dimensional flow around square and circular piers." *Int. J. Numer. Methods Fluids* 34 (3): 207 227. https://doi.org/10.1002/1097 0363(20001015)34:3<207::AID FLD31>3.0.CO;2 R.

Uchida, T., S. Fukuoka, A. T. N. Papanicolaou, and A. G. Tsakiris. 2016. "Nonhydrostatic quasi 3D model coupled with the dynamic rough wall law for simulating flow over a rough bed with submerged boulders." *J. Hydraul. Eng.* 142 (11): 04016054. https://doi.org/10.1061/(ASCE)HY.1943 7900.0001198.

Wang, H., and H. Chanson. 2018. "Modelling upstream fish passage in standard box culverts: Interplay between turbulence, fish kinematics, and energetics." *River Res. Appl.* 34 (3): 244 252. https://doi.org/10.1002/rra.3245.

Yu, G., E. J. Avital, and J. J. Williams. 2008. "Large eddy simulation of flow past free surface piercing circular cylinders." *J. Fluids Eng.* 130 (10): 101304. https://doi.org/10.1115/1.2969462.

Zhou, Y., H. J. Zhang, and M. W. Yiu. 2002. "The turbulent wake of two side by side circular cylinders." *J. Fluid Mech.* 458 (May): 303 332. https://doi.org/10.1017/S0022112002007887.

Ziada, S. 2006. "Vorticity shedding and acoustic resonance in tube bundles." *J. Braz. Soc. Mech. Sci. Eng.* 28 (2): 186 189. https://doi.org/10.1590/S1678 58782006000200008.